Progress In Electromagnetics Research B, Vol. 106, 151-165, 2024 PIER B

(Received 14 April 2024, Accepted 16 June 2024, Scheduled 23 June 2024)

Equivalent Circuit Model of Antenna Array Utilizing an Archimedean Spiral Sequential Feed Network for C-Band Applications

Khalid S. Ahmad[1,2], Fauziahanim C. Seman[1], Shipun A. Hamzah[1], Khaled Alhassoon[3], Tale Saeidi[4], Zahriladha Zakaria[5], and Ahmed Jamal Abdullah Al-Gburi[5,*]

[1]*Research Center for Applied Electromagnetic (EMCenter), Institute of Integrated Engineering Universiti Tun Hussein Onn Malaysia, Parit Raja 86400, Malaysia*
[2]*Department of Electronic Engineering, Mosul Technical Institute Northern Technical University (NTU), Al-Majmoaa street, Mosul, Iraq*
[3]*Department of Electrical Engineering, College of Engineering, Qassim University, Buraydah 52571, Saudi Arabia*
[4]*WiSAR Lab, Atlantic Technological University (ATU), Letterkenny, Co. Donegal F92 FC93, Ireland*
[5]*Center for Telecommunication Research & Innovation (CeTRI), Faculty of Electronics and Computer Technology and Engineering Universiti Teknikal Malaysia Melaka (UTeM), Jalan Hang Tuah Jaya, Durian Tunggal, Melaka 76100, Malaysia*

ABSTRACT: This paper introduces the configuration of a microstrip antenna array with a new Archimedean spiral sequential feed network (SSFN) for the upper half of the C-band application. The Archimedean SSFN mechanism uses four circular patch elements to structure the proposed antenna array. The optimized reflection loss (S_{11}) of the proposed SSFN mechanism was obtained by tuning the dimensions of each transformer and then connected with an antenna array. Aiming to make the suggested antenna array compact in size, bending feed lines were utilized. The antenna array is designed with the overall physical dimensions of 75 mm × 75 mm × 1.575 mm, with an electrical size of $1.85\lambda_o$ mm, $1.85\lambda_o$ mm, $0.038\lambda_o$ at a frequency of 7.43 GHz. An equivalent circuit model (ECM) is designed and analyzed to verify the proposed Archimedean SSFN and the designed antenna array. Reflection losses of SSFN and microstrip spiral antenna array (SAA) were confirmed with the suggested circuit model utilizing Computer Simulation Technology (CST) Microwave Studio and Applied Wave Research (AWR) Microwave Office software. According to the empirical results, the SAA has a reflection loss bandwidth of 2.08 GHz (6.15–8.23 GHz) and a maximum gain of 10.2 dBi at 7.43 GHz. The axial ratio (AR) of the proposed antenna covers a bandwidth of 1.6 GHz (6.2–7.8 GHz), which is approximately 22.85% of the entire bandwidth. These results demonstrate a perfect agreement between the simulated and measured outcomes, making the suggested SAA suitable for the C-band wireless application.

1. INTRODUCTION

With the latest continuing advance in communications, circularly polarized (CP) radiators have obtained [1] significant interest due to their attractive characteristics for non-line-of-sight purposes, supplying better moving than linearly polarized radiators, and they have been extensively utilized in satellite, radar, and portable communication equipment [2, 3].

Microstrip technology is the preferred choice for many implementations for its attractive properties, small dimension, light weight, and low cost [4, 5]. Corporate microstrip feed network is utilized to feed the antenna elements. Unfortunately, the number of discontinuities is significantly high, thus increasing feed loss and pattern disturbance [6]. On the other hand, series sequential feed network (SFN) has smooth bends, a high transmission line impedance [7], and low complexity, and is the best solution to reduce discontinuities, feed losses, and pattern disturbance [6]. Various configurations of CP antenna arrays are suggested, but sequential feed mechanism is one of the most popular methods explored in the literature to produce CP implementation [2, 3, 8–14].

SFN technique, which was first characterized by Hall et al. [15], is an interesting technique and has been used extensively for patch arrays to improve cross-polarization rejection in the main beam [1], increase bandwidth, improve input voltage standing wave ratio (VSWR) [16] and gain [17]. In [2, 3], many methods have been proposed for different applications [8–12, 14, 18, 19]. In [3], a sequentially rotated network feeds four Archimedean spiral elements integrated with a circular slot at the back of each antenna. The feed network used a branch line, 90°, and a rat-race coupler, 180°, to achieve the required phase distributions. Moreover, a cavity-backed structure integrated with each antenna improves the peak gain and realizes a directional radiation pattern, but the array size increases. In [20], a feed network consists of three transmission lines as phase-shifting power dividers and four additional transmission lines that provide impedance transformation between the network outputs and the antenna input ports. This work proposed a circular patch with an elliptical cut in the center as an element. In [21], an array comprises 2×2 elements fed

* Corresponding author: Ahmed Jamal Abdullah Al-Gburi (ahmedjamal@ieee.org) and (engahmed_jamall@yahoo.com).

by a sequential rotation network. The feeding network contains three T-junction sections, one anti-phase delay line and two 90-phase delay lines, with phase distributions of 0, 90, 180, and 270 degrees. The element used is a slot antenna equipped with 4×4 EBG unit cells. In this study [22], researchers develope a 2×2 sequentially rotating antenna array as a feedline and utilize circular-arc feedlines to minimize discontinuity and reduce loss within the feeding network. Each element is excited by a corporate microstrip feed network, which controls phase and impedance matching. In [23], a sequential feed network consists of seven quarter-wave transformer sections curved and linked in a consecutive sequence to form a four-port network. Four antennas are used, and each antenna is constituted from a square aperture with a ground-plane conductor and excited with a rectangular patch [24]. The suggested four-ring slot antennas are fed by a sequentially rotating network. Four slots are inserted on the ground plane to enhance antenna array performance. These slots compensate the gain decline when the antenna height decreases.

SFN is capable of feeding only a circle-shaped antenna array. Here, an alternative technique is proposed: spiral sequential feed network (SSFN) instead of the (circular) SFN. The reason for SSFN is to feed spiral antenna array (SAA), and this technique can also be used to feed circular antenna array. Previous analysis displayed that the spiral arrangement of the antenna provides good results in the radiation pattern like low-level side lobes and a narrow main lobe [25].

In this article, a CP SAA is presented, employing an SSFN technique. To arrange the SAA, an Archimedean SSFN is utilized to excite the single elements separately for application in the frequency band (6.14–8) GHz. The feed network is optimized by using CST Microwave Studio (CST MWS) in terms of providing convenient power splitting and phase shifting at output ports. The results show that the proposed SSFN is able to provide power splitting and phases at the output ports similar to the common SFN and are usually oriented sequentially at 0°, 90°, 180°, and 270°.

2. THE PROPOSED SSFN DESIGN

2.1. The SSFN with Straight Feed Lines (SFL)

The SSFN shown in Fig. 1 is similar to SFN, consisting of seven quarter-wave transformers. (T_1–T_7) represents the numbering of transformers. Table 1 illustrates the dimensions and impedance of each transformer. T_2, T_4, and T_6 at first look like to have circular-like common shapes [13, 20], but in fact, they are Archimedean spiral shapes. The following equations are the general form for generating these three transformers in a Cartesian coordinate system.

$$x(t) = a_t \cos t, \quad (1)$$
$$y(t) = a_t \sin t, \quad (2)$$

where a and t are constant and angle, respectively, while $r(t)$ is the radius of the spiral shape in the polar coordinate system.

$$r(t) = a_t. \quad (3)$$

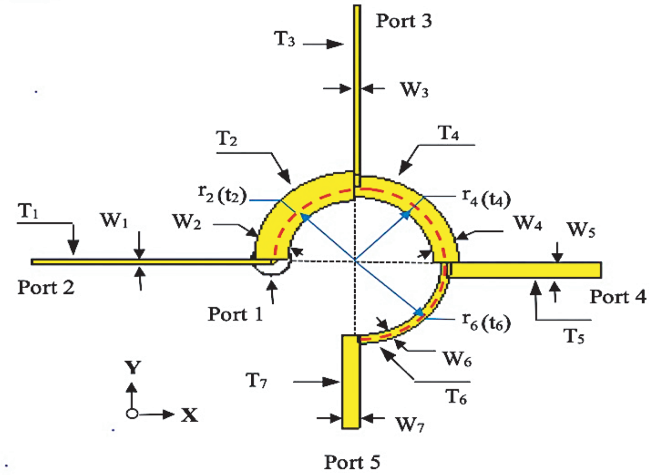

FIGURE 1. The SSFN configuration.

For T_2

$$x_2(t_2) = 0.099t_2 \cos t_2, \quad (4)$$
$$y_2(t_2) = 0.099t_2 \sin t_2, \quad (5)$$

where t_2, $45\pi/2 \le t2 \le 46\pi/2$.

For T_4

$$x_4(t_4) = 0.0999t_4 \cos t_4, \quad (6)$$
$$y_4(t_4) = 0.0999t_4 \sin t_4, \quad (7)$$

where t_4, $46\pi/2 \le t4 \le 47\pi/2$.

For T_6

$$x_6(t_6) = 0.105t_6 \cos t_6, \quad (8)$$
$$y_6(t_6) = 0.105t_6 \sin t_6, \quad (9)$$

where t_6, $47 * \pi/2 \le t6 \le 48 * \pi/2$.

The radii of T_2, T_4, and T_6 are r_2 (t_2), r_4 (t_4), and r_6 (t_6), respectively.

$$r_2(t_2) = 0.099t_2, \quad (10)$$
$$r_4(t_4) = 0.0999t_4, \quad (11)$$
$$r_6(t_6) = 0.105t_6, \quad (12)$$

It is necessary that the width of the feed network T_1, T_3, T_5, and T_7 is as narrow as practically possible [7, 27] to minimize spurious radiation and coupling impacts, as shown in Table 1 and Fig. 1. Figs. 2(a), (b), and (c) display the reflection loss

TABLE 1. Modulating the widths, lengths, and characteristic impedance of each transformer in SSFN.

Transformer No.	W (mm)	L (mm)	Z (1 to 7) (Ω)
T_1	0.5923	20.227	134.81
T_2	2.857	29.91	68.99
T_3	0.5696	17.863	136.43
T_4	2.135	30.16	80.59
T_5	1.4812	13.133	95.85
T_6	0.82155	30.68	121.01
T_7	1.4812	9.133	95.85

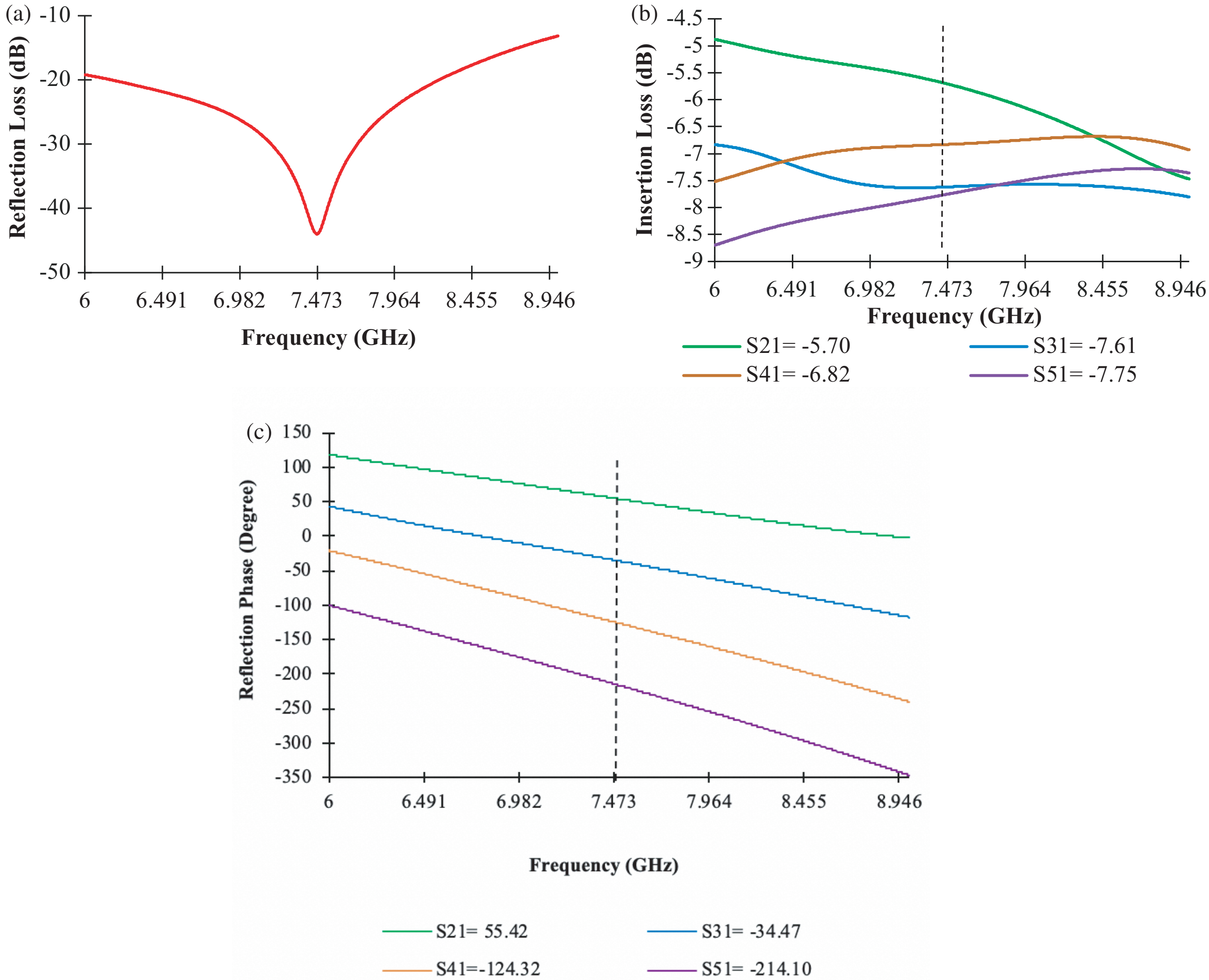

FIGURE 2. The simulated results of SSFN with SFL. (a) Reflection loss. (b) Magnitudes. (c) Phase difference.

at port 1, and magnitudes and phases at ports 2, 3, 4, and 5, respectively, at 7.473 GHz. The proposed network provides a reflection loss ($11 > -43.9$ dB), as displayed in Fig. 2(a). Fig. 2(b) displays a balanced distribution of the power magnitude at the output ports (6.7 ± 1 dB). In addition to their service as an impedance transformer, T_1–T_7 provide a phase difference of 90° among output ports 2, 3, 4, and 5, according to Fig. 2(c) and as mentioned in [27]. Fig. 2(c) displays the simulated output phase. This network provides feed phases of (89.89°, 89.85°, and 89.78°) at 7.473 GHz and provides relative feed phases of 90° at ports 2–5 for other frequencies between 6 and 9 GHz.

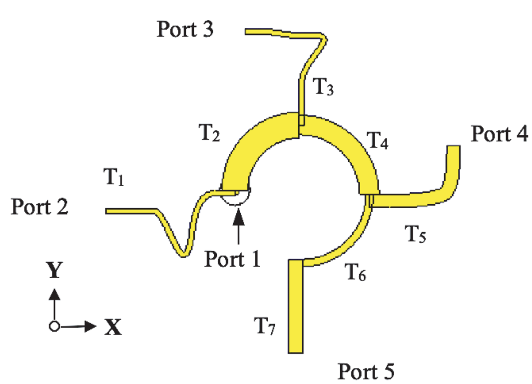

FIGURE 3. The compact SSFN configuration.

2.2. Compact SSFN

In order to make the proposed SSFN with a compact shape, and hence compact SAA, the transformers (feed lines) T_1, T_3, and T_5 were changed from straight lines to bending lines, as seen in Fig. 3.

Figures 4(a), (b), and (c) show the reflection loss at port 1, magnitudes, and phases at ports 2, 3, 4, and 5, respectively, at 7.419 GHz. Fig. 4(a) shows that the maximum reflection loss of the compact network shifted about 54 MHz downwards from 7.473 GHz with a reflection loss of -43.9 dB to 7.419 GHz with a reflection loss of -41 dB, compared with SSFN using SFL shown before in Fig. 2(a), due to employing bending feed lines. Fig. 4(b) shows a balanced distribution of the power magnitude on the output ports (7.4 ± 0.6 dB). Fig. 4(c) displays the simulated output phase. This network produces feed phases of

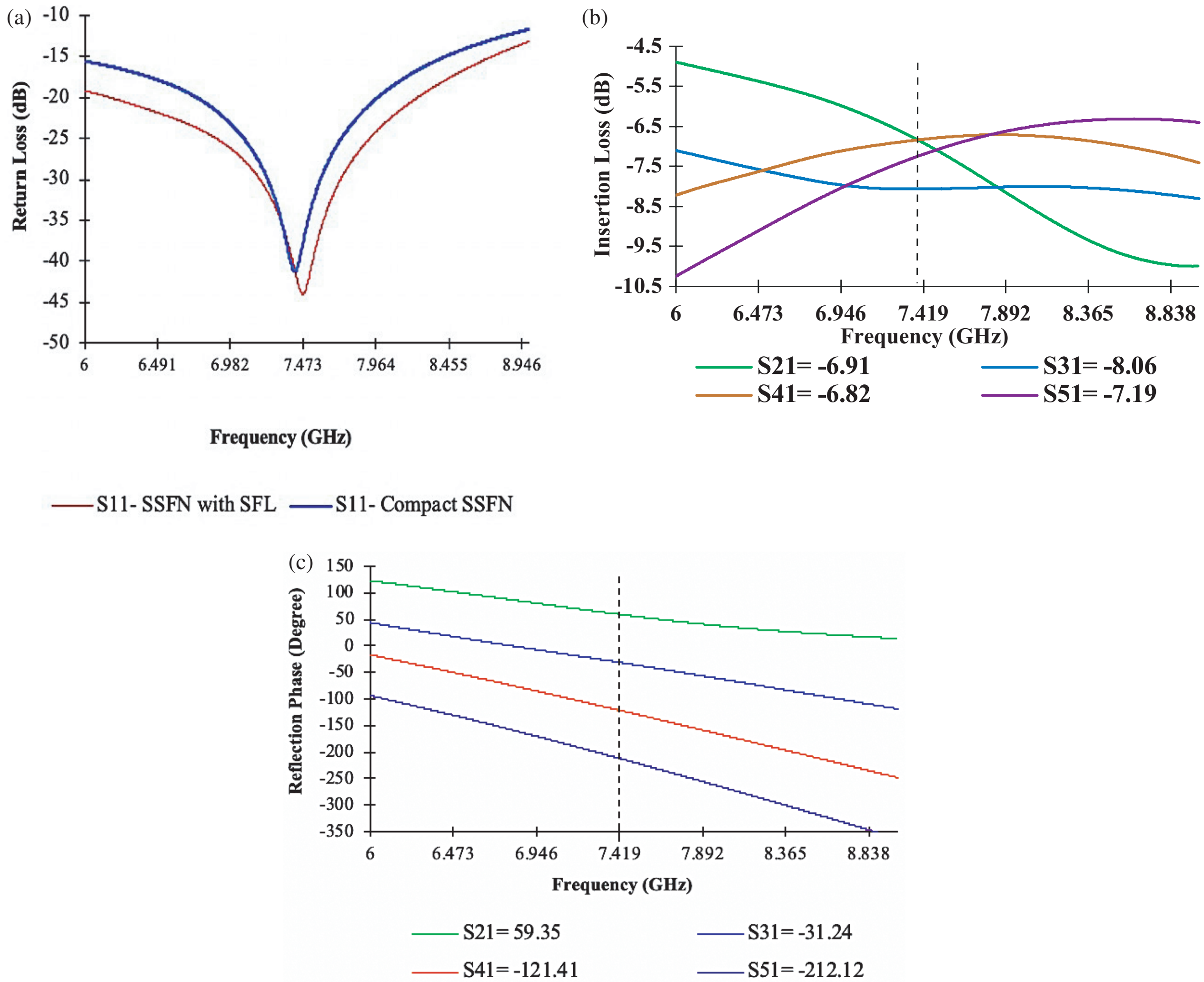

FIGURE 4. The simulated outcomes of the compact SSFN, including (a) reflection loss, (b) magnitudes, and (c) phase difference.

(90.59°, 90.17° and 90.71°) at 7.419 GHz, and provides relative feed phases of 90° at the antenna ports 2–5 for other frequencies between 6 and 9 GHz.

For preparing the design for fabrication, it is necessary to reduce the size of the board, as seen in Fig. 5(a), and the fabricated prototype is shown in Fig. 5(b). The replacement of the waveguide ports with SMA ports is shown in Fig. 5(c), and a photo of the manufactured prototype is displayed in Fig. 5(d). It is observed that by reducing the board size, the frequency shifted 19 MHz downwards, from 7.419 GHz with a reflection loss of -41.21 dB (Fig. 4(a)) to 7.40 GHz with a reflection loss of -45.12 dB, as seen in Fig. 6. Furthermore, by changing waveguide ports to SMA ports, the frequency shifted 610 MHz upwards from 7.40 GHz to 8.01 GHz with a reflection loss of -34.9 dB, as shown in Fig. 6. For validation purposes, a compact SSFN has been fabricated based on the geometrical dimensions, which were realized on RT/Duroid 5880 ($\varepsilon_r = 2.2$, loss tangent $= 0.009$, substrate thickness $= 1.575$ mm, and copper thickness $= 0.035$ µm). The maximum reflection loss was centered at 8.09 GHz, with a reflection loss of -20.68 dB, as seen in Fig. 6.

As a comparison between Fig. 4 and Fig. 7, the simulated balanced distribution and phase difference at the output ports slightly changed due to using the SMA port and board reduction. The differentiation among simulated and measured balanced distributions and phase difference (SSFN with SMA) at 8.01 GHz is shown in Fig. 7 and Table 2. The simulated results of the (SSFN with SMA) provide feed phases of (109.26°, 83.37°, and 98.28°) at the operating frequency of 8.01 GHz. Further, the measured results provide feed phases of (111.72°, 69.9°, and 108.4°) at the same operating frequency. One

TABLE 2. Contrasting simulated and measured magnitudes and phase differences at the output ports at a frequency of 8.01 GHz.

S-parameters	Magnitude (dB)		Phase difference (dB)	
	simulated	measured	simulated	measured
S_{21}	8.55	9.11	-19.32	-25.19
S_{31}	9.19	9.06	-128.58	-136.91
S_{41}	4.08	4.12	-211.95	-206.81
S_{51}	10.61	11.11	-310.23	-315.21

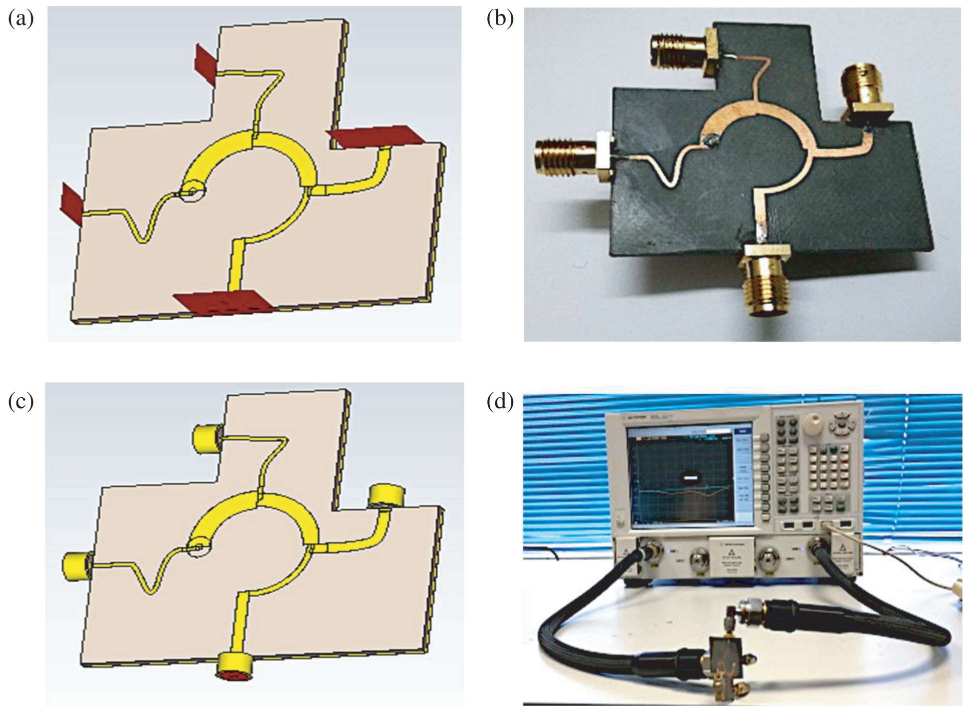

FIGURE 5. (a) SSFN design with waveguide ports using CST software, (b) image of the SSFN prototype, (c) SSFN design with SMA ports, and (d) image of the SSFN prototype undergoing testing within the measurement setup using a VNA.

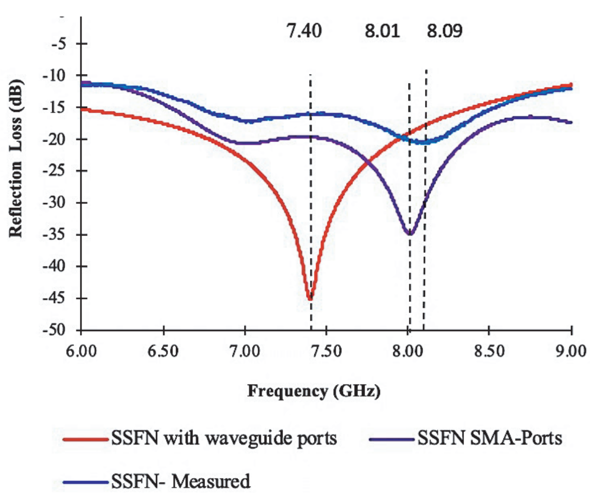

FIGURE 6. Contrasting the reflection loss between simulated and measured values.

can observe an excellent agreement between simulated and measured results. For the remaining frequencies in the 6–9 GHz range, the measured transmission phases were somewhat shifted compared to the simulated values due to the difference in the length of the coaxial line between the measurement and simulation.

2.3. ECM for the Compact SSFN

The ECM was designed and analyzed in this study using Applied Wave Research (AWR) software. Many researchers have developed an ECM as suggested in [12, 19, 26]. However, they used complicated methods and investigations. This work simply explains the ECM by using the model for a rectangular patch antenna to extract the equivalent model for each $\lambda/4$ transformer in SSFN.

A simple idea has been proposed based on using the ECM for a rectangular patch antenna to extract the ECM for each $\lambda/4$ transformer in SSFN. Each transformer is represented by a parallel Cp, Lp, Rp circuit, where Cp, Lp, and Rp are the equivalent capacitance, inductance, and resistance, respectively. This model takes into account the physical parameters of the shape. The equivalent lumped element of the transformers has been evolved using the cavity model. The values of Cp, Lp, and Rp are determined as follows [28].

$$C_p = \frac{\varepsilon_{eff}\varepsilon_0 LW}{2h}\cos^{-2}\left(\frac{\pi_{y_0}}{L}\right)(F) \tag{13}$$

$$L_p = \frac{1}{C_p\omega_r^2}(H) \tag{14}$$

$$R_p = \frac{Q_r}{C_p\omega_r}(\Omega) \tag{15}$$

$$Q_r = \frac{v\left(\varepsilon_{\mathit{eff}}\right)^{1/2}}{4f_r h} \tag{16}$$

where $\varepsilon_{\mathit{eff}}$ is the effective relative permittivity; ε_0 is the relative permittivity of free-space ($\varepsilon_0 = 1/v^2\mu_0$), $\varepsilon_0 = 8.85 \times 10^{-12}\,\mathrm{F}\cdot\mathrm{m}^{-1}$; v is the speed of electromagnetic waves in free space; W and L denote the width and length of the transformer, respectively; y_0 is the inset-fed point location for patch antenna,

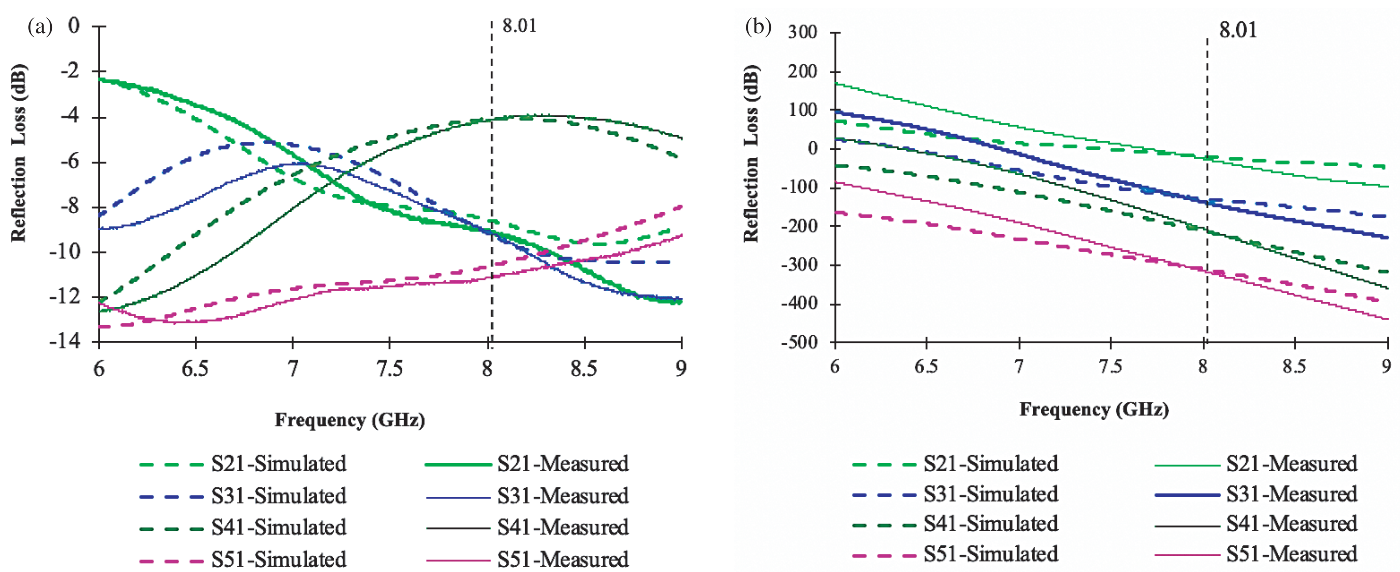

FIGURE 7. Comparison among simulated and measured (a) magnitudes and (b) phase differences.

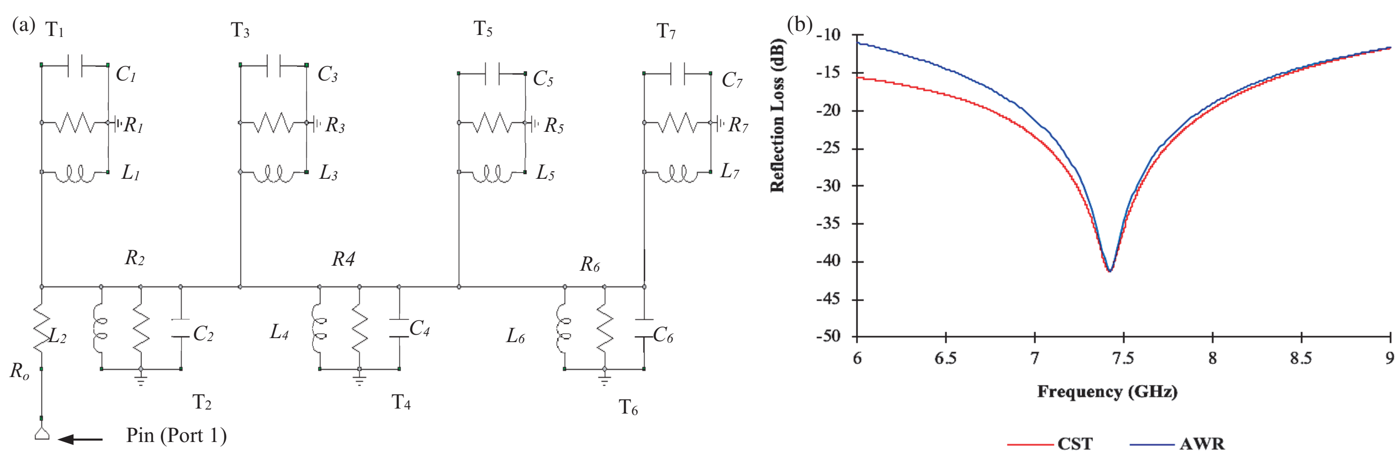

FIGURE 8. (a) Equivalent circuit of the compact SSFN $C_1 = 0.0573\,\mathrm{pF}$, $R_1 = 3133\,\Omega$, $L_1 = 8.020\,\mathrm{nH}$, $C_2 = 0.4363\,\mathrm{pF}$, $R_2 = 425.4\,\Omega$, $L_2 = 1.054\,\mathrm{nH}$, $C_3 = 0.0486\,\mathrm{pF}$, $R_3 = 3691\,\Omega$, $L_3 = 9.455\,\mathrm{nH}$, $C_4 = -0.324\,\mathrm{pF}$, $R_4 = 568.6\,\Omega$, $L_4 = 1.4202\,\mathrm{nH}$, $C_5 = 0.0962\,\mathrm{pF}$, $R_5 = 1898\,\Omega$, $L_5 = 4.779\,\mathrm{nH}$, $C_6 = 0.1219\,\mathrm{pF}$, $R_6 = 1481\,\Omega$, $L_6 = 3.772\,\mathrm{nH}$, $C_7 = 0.0669\,\mathrm{pF}$, $R_7 = 2729\,\Omega$, $L_7 = 6.872\,\mathrm{nH}$, $R_o = 12.8\,\Omega$, (b) The reflection loss for network, simulated with both software packages.

whereas in this research, y_0 equals zero; h is the thickness of the board; ω_r and Q_r are the angular frequency at resonance [28] and the radiation quality factor, respectively [29]. The resonant frequency is taken to be 7.419 GHz, the frequency of the maximum reflection loss of the compact SSFN.

The ECM for each transformer is connected in series with ECM for the other transformers. Fig. 8(a) illustrates the equivalent circuit for the proposed SSFN. Furthermore, there are a few losses symbolized by series $R_o = 12.8\,\Omega$. It symbolizes further losses in the ECM. It has been introduced as a parameter to supply a closer agreement among the suggested ECM and simulation results. It is worth mentioning here how to calculate the equivalent circuit of the convex transformers T_2, T_4, and T_6 and the bending transformers T_1, T_3, and T_5. The method is based on the calculation of the length of the spiral arc or bend transformers, then dealing with these transformers as straight forms. Fig. 8(b) displays the comparison among reflection losses of the compact SSFN simulated in CST MWS and the SSFN model circuit simulated by the AWR-Microwave Office. The maximum reflection loss of the CST MWS curve was observed at 7.419 GHz, while the AWR curve was 7.42 GHz. The two curves are in good agreement. The difference in bandwidth (BW) between the two curves, owing to numerical analysis in AWR, does not take in account the bending feed lines as well as curving in T_2, T_4, and T_6.

3. THE SAA DESIGN

A set of 2×2 spiral-based patch elements has been connected to the compact SSFN through ports 2, 3, 4, and 5. The spiral shape of the proposed SSFN will impose a new form of array

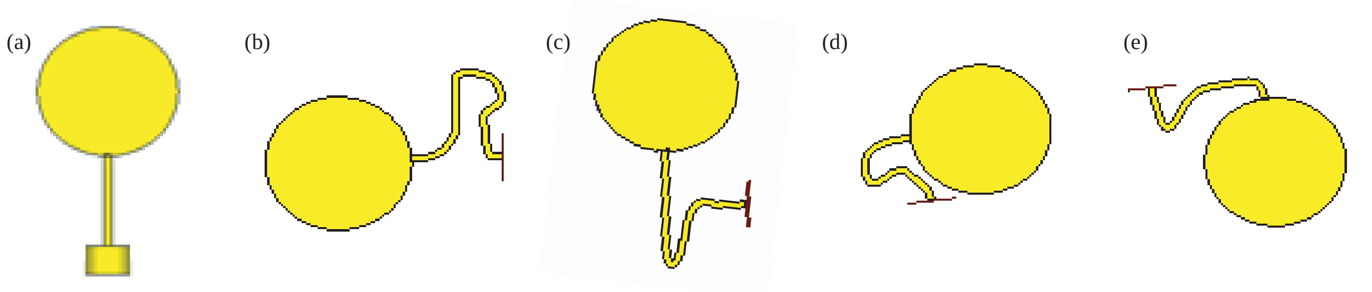

FIGURE 9. Comparison among antenna feed line designs, (a) antenna with SFL, (b) antenna 1 linked to port 2, (c) antenna 2 linked to port 3, (d) antenna 3 linked to port 4, (e) antenna 4 linked to port 5.

configuration, which is the arrangement of the spiral elements. Further, the new spiral feed network or SSFN can be used for feeding a circular array. Owing to the Archimedean spiral antenna arrangement, the remaining distance between patches and ports is not equal like with a circular array, which is why this paper proposed different feed line bending for each element, while in the circular antenna array, all feed lines have similar bending shape [7, 8, 12, 13, 18–20, 27].

The element radius and feed line width were adopted as 6.86 mm and 0.66 mm, respectively. Fig. 9(a) shows the circular patch with SFL before the bending process, which resonates at 7.482 GHz. Figs. 9(b), (c), (d), and (e) show the antenna feed lines shape which will connect to ports 2, 3, 4, and 5, respectively. The resonance frequency of the patches was adjusted to match the resonance frequency of the maximum reflection loss of the compact SSFN at 7.419 GHz, by choosing the proper bend shape. It was observed from simulated results that changing the shape of bending leads to shifting the resonance of element upward or downward, in addition to changing the value of reflection loss.

The characteristics impedance of the antenna with very low reflection loss will definitely be close to 50 Ω with a reduction in side lobe level as observed through simulation results. Fig. 10 displays the comparison between the reflection loss of circular patch with SFL vs. the reflection loss for the other elements in the array and the reflection loss for compact SSFN.

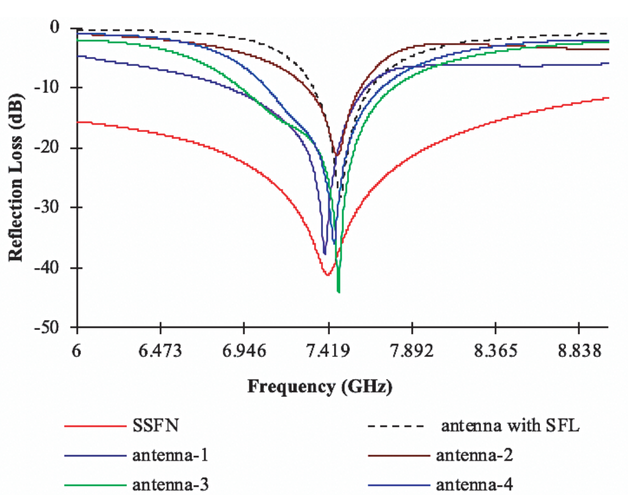

FIGURE 10. Simulated reflection losses for compact SSFN, patch with SFL, and antenna 1, 2, 3, and 4 in SAA.

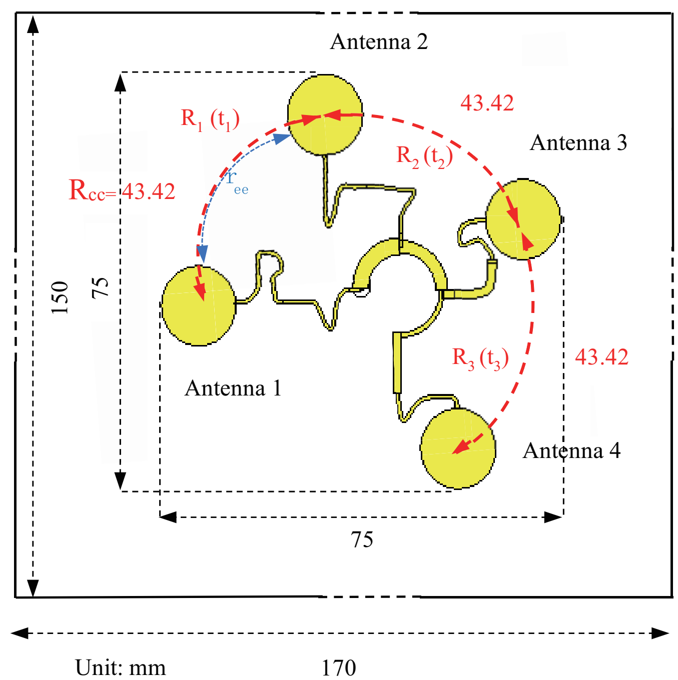

FIGURE 11. The proposed SAA configuration with Rcc 43.42 mm.

Figure 11 shows the geometry of the SAA, the array arranged in a 75 mm × 75 mm square ($1.85\lambda_o^2$ at 7.419 GHz). The board size is 170 mm × 150 mm. All circular patches have an equal radius of 6.86 mm. The separation distances between elements from edge to edge (r_{ee}) are kept at 29.7 mm ($0.73\lambda_o$ at 7.419 GHz). The spiral arc length used for arranging patches is 43.42 mm ($1.07\lambda_o$), where the length of the arc was calculated on the basis of the space between two neighbouring antennas from centre to centre (R_{cc}). R_1 (t_1), R_2 (t_2), and R_3 (t_3) represent the radii of the spiral path. The reason for adopting Rogers board 5880, loss tangent 0.009, thickness 1.575 mm with a low dielectric constant 2.2 is because a small dielectric constant is preferred to obtain a good axial ratio for CP application [30] in the case of using the same circular patch with a concentric elliptical cut to generate CP [13].

$$R_1\left(t_1\right) = 0.95t_1 \tag{17}$$

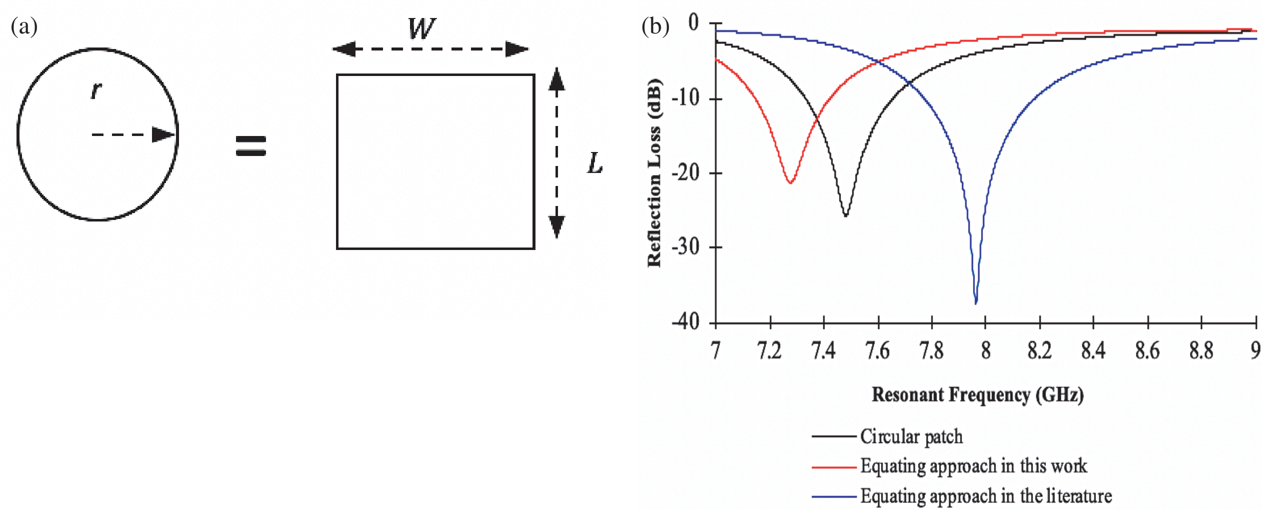

FIGURE 12. (a) Graphical diagram for equating the area of circular patch with square patch. (b) Comparison among the circular patch vs. the equating in this paper and in [32, 33].

where t_1, $20\pi/2 \leq t_1 \leq 20.9054\pi/2$

$$R_2(t_2) = 0.98t_2 \tag{18}$$

where t_2, $20.9435\pi/2 \leq t_2 \leq 21.7837\pi/2$

$$R_3(t_3) = 1.01t_3 \tag{19}$$

where t_3, $21.8123\pi/2 \leq t_3 \leq 22.5967\pi/2$.

The values of the spiral path radii depend on the available space around SSFN. As seen from Fig. 11, the SAA is based on a compact SSFN applied to set 2×2 compact antenna elements, where the antenna feed lines based on space-filling ability are arranged to fit the area between the antennas.

The coaxial probe of $50\,\Omega$ is employed in a simulation. Simulation works have been done employing frequency domain solver in CST MWS with open (add space) boundary conditions.

3.1. ECM for the SAA

The ECM for a circular patch can be described as a parallel set of R, L, and C similar to a rectangular patch. However, the approach used in [31] is complicated. Aiming to simplify this approach, this article proposed a new simple approach based on employing [29, 31–33] used previously. It is based on equating the circular area of the microstrip circular patch to the square microstrip patch. A circular patch of diameter $2r$ is considered as a square patch of width W and length of L. The width and length of the corresponding square patch are computed by equating the root of the circular area schematic, as seen in Fig. 12(a), where the radius of the circular patch is $r = 6.86$ mm, and the area of the circular patch is $A = 147.84\,\text{mm}^2$. The root of circular patch area is 12.158 mm, which represents the W and L of square patch radiator. It is clear from (20) and (21) that multiplying W by L equals 7.81 mm, approximately equal to the area of the circular patch. The following formulas have been used for extracting the dimensions of the square patch.

$$A = \pi r^2 \tag{20}$$

$$W = L = \sqrt{A} \tag{21}$$

In [32, 33], another approach has been used for equating circular patch area, where W and L are represented as $2r$ and $\pi r/2$, respectively. As illustrated earlier in Fig. 10, the resonant frequency of circular element in the array is adopted to be around 7.419 GHz for the element with a bending feed line for a patch radius of 6.86 mm because it should be similar to the frequency of the maximum reflection loss of the compact SSFN. In this section, the calculation has been done with SFL, thus the circular patch with the same mentioned radius resonates at resonant frequency 7.482 GHz with a shift 63 MHz upwards. The Equivalent Circuit Model (ECM) for a circular patch can be described as a parallel set of R, L, and C, similar to a rectangular patch. However, the approach used in [31] is complicated. To simplify this approach, this article proposes a new, simpler method based on the techniques previously employed in [29, 31–33]. Fig. 12(b) displays the comparison between reflection loss curves for the circular patch vs. the proposed approach used in this work and the approach used in [32, 33], where they resonate at 7.482 GHz, 7.276 GHz, and 7.964 GHz, respectively. The simulation comparison has been done for the same length and width of feed lines 9.75 mm and 0.66 mm, respectively. The -10 dB of the circular patch is 318 MHz while for the approach in this work and in [32, 33] they are 274 MHz and 404 MHz, respectively. The difference between resonant frequency for the circular patch and the approach in this work is 2.75%, while for the approach in [32, 33] it is 6.44%.

To prove the validity of the new equating approach, Table 3 shows the difference between the resonant frequencies for the circular and square patches (after equating approach) at different frequencies 7 GHz, 8.5 GHz, 10 GHz, and 12 GHz, where the difference between the two resonant frequencies remains

TABLE 3. The comparison between circular and square patch.

Circular patch frequency (GHz)	Square patch frequency (GHz)	Difference (%)
7	6.828	2.45
8.5	8.32	2.11
10	9.788	2.12
12	11.688	2.6

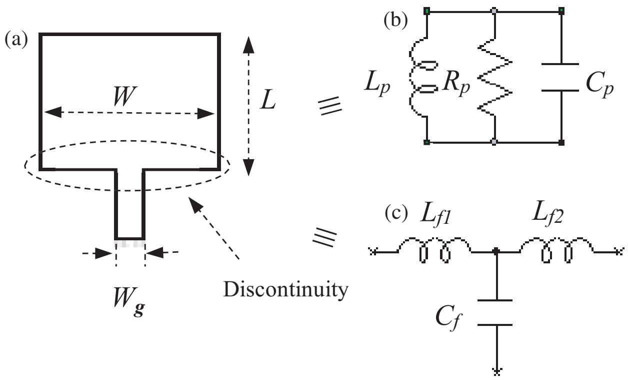

FIGURE 13. Geometry of single rectangular element and step discontinuity. (a) Shape. (b) Patch circuit model with $L_p = 0.5609\,\text{nH}$, $R_p = 235.89\,\Omega$, $C_p = 0.8203\,\text{pF}$. (c) Feed circuit model with $L_{f1} = 0.00016844\,\text{pH}$, $L_{f2} = 0.00080099\,\text{pH}$, $C_f = 0.000000084060\,\text{pF}$.

almost constant between 2.1% and 2.6% in reasonable proportions.

The circuit model for a square patch without a feed line is represented as parallel (C_p, L_p, R_p) [28], as seen in Fig. 13(b). The amounts of C_p, L_p, and R_p can be computed from (17) to (20), where W and L symbolize the width and length of a square patch, respectively. There is a sharp variation in line width at the intersection of the patch and feed line, which is called a discontinuity. The discontinuity is seen in Fig. 13(a), and it is caused by an unexpected variation in the geometry of the strip conductor, where W is the width of the wide microstrip portion, and Wg is the width of the narrow line portion. It should be noted that the discontinuity causes reflections of the signal with a few radiations. The charges will become greater on the conductor due to electric charges that head to collect at the boundaries of a discontinuity. As a result, the electric field rises, and electric energy is stocked. The resulting impact can be symbolized as a capacitive C_f in the circuit model [34], as seen in Fig. 13(c). C_f symbolizes the fringing field capacitance at the intersection [34, 35]. The discontinuity regulates the allocation of the current and grows the magnetic field. Magnetic energy is stocked in higher-order modes that make an inductive effect, which can be symbolized as L_{f1} and L_{f2} in ECM [34], as seen in Fig. 13(c). Thus, C_f, L_{f1}, and L_{f2} are the equivalent capacitance and inductance of the feed transmission line (TL) and discontinuity. C_f is presented as [29].

$$C_f = 0.00137h\frac{(\varepsilon_{\mathit{eff1}})^{1/2}}{Z_{c1}}\left(1-\frac{W_g}{W}\right)$$

$$\cdot\left(\frac{\varepsilon_{\mathit{eff1}}+0.3}{\varepsilon_{\mathit{eff1}}-0.258}\right)\left(\frac{\frac{W_g}{h}+0.264}{\frac{W_g}{h}+0.8}\right), \tag{22}$$

$$\varepsilon_{\mathit{eff1}} = \frac{\varepsilon_r+1}{2}+\frac{\varepsilon_r-1}{2}\frac{1}{\left(1+12\frac{h}{W}\right)^{1/2}}, \tag{23}$$

$$Z_{c1} = 120\pi\left(\varepsilon_{\mathit{eff1}}\right)^{-1/2}$$

$$\cdot\frac{1}{\left(\frac{W}{h}+1.393+0.667\ln\left(\frac{W}{h}+1.444\right)\right)}, \quad (\Omega) \tag{24}$$

where $\varepsilon_{\mathit{eff1}}$ and Z_{c1} are the effective relative permittivity and characteristic impedance of square patch, respectively. ε_{eff1} depends on the board thickness, h, and conductor width W. L_{f1} and L_{f2} can be calculated from the following equations [34–36].

$$L_{f1} = \frac{L_{w1}}{L_{w1}+L_{w2}}L_d, \quad (\text{nH}) \tag{25}$$

$$L_{f2} = \frac{L_{w2}}{L_{w1}+L_{w2}}L_d, \quad (\text{nH}) \tag{26}$$

L_{w1} and L_{w2} are inductive per unit length of the square patch and feed line, having widths of W and Wg, respectively, while L_d is the overall discontinuity inductance and presented by [34–36].

$$L_{w1} = Z_{c1}\frac{(\varepsilon_{\mathit{eff1}})^{1/2}}{v}, \quad (\text{H/unit length}) \tag{27}$$

$$L_{w2} = Z_{c2}\frac{(\varepsilon_{\mathit{eff2}})^{1/2}}{v}, \quad (\text{H/unit length}) \tag{28}$$

where $\varepsilon_{\mathit{eff2}}$ and Z_{c2} are the effective relative permittivity and characteristic impedance of the feed line, respectively. The resonant frequency is taken to be 7.419 GHz. The units of length employed in equations are metres

$$\varepsilon_{\mathit{eff2}} = \frac{\varepsilon_r+1}{2}+\frac{\varepsilon_r-1}{2}\frac{1}{\left(1+12\frac{h}{W_g}\right)^{1/2}}, \tag{29}$$

$$Z_{c2} = 120\pi\left(\varepsilon_{\mathit{eff2}}\right)^{-1/2}$$

$$\cdot\frac{1}{\left(\frac{W_g}{h}+1.393+0.667\ln\left(\frac{W_g}{h}+1.444\right)\right)}, \quad (\Omega) \tag{30}$$

$$L_d = 0.000987h\left(1-\frac{Z_{c1}}{Z_{c2}}\left(\frac{\varepsilon_{\mathit{eff1}}}{\varepsilon_{\mathit{eff2}}}\right)^{1/2}\right) \tag{31}$$

Figure 14(a) symbolizes the ECM for the suggested SAA, four patches connected with SSFN. Fig. 14(b) displays the comparison between reflection losses of the array simulated in CST MWS and the array circuit model simulated by AWR-Microwave Office. The minimum reflection loss of the CST MWS curve was observed at 7.437 GHz, and their $-10\,\text{dB}$

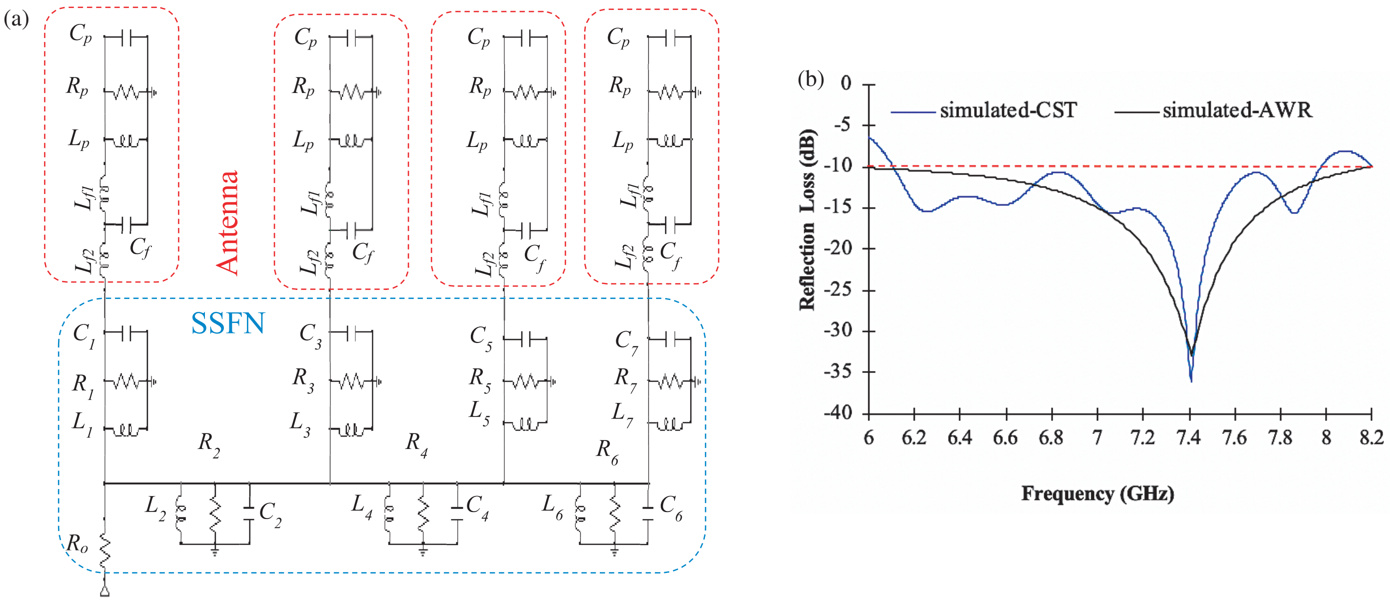

FIGURE 14. (a) The equivalent circuit of SAA $C_p = 0.8203\,\text{pF}$, $R_p = 235.89\,\Omega$, $L_p = 0.5609\,\text{nH}$, $L_{f1} = 0.00016844\,\text{pH}$, $L_{f2} = 0.00080099\,\text{pH}$, $C_f = 0.000000084060\,\text{pF}$, $C_1 = 0.0573\,\text{pF}$, $R_1 = 3133\,\Omega$, $L_1 = 8.020\,\text{nH}$, $C_2 = 0.4363\,\text{pF}$, $R_2 = 425.4\,\Omega$, $L_2 = 1.054\,\text{nH}$, $C_3 = 0.0486\,\text{pF}$, $R_3 = 3691\,\Omega$, $L_3 = 9.455\,\text{nH}$, $C_4 = 0.324\,\text{pF}$, $R_4 = 568.6\,\Omega$, $L_4 = 1.4202\,\text{nH}$, $C_5 = 0.0962\,\text{pF}$, $R_5 = 1898\,\Omega$, $L_5 = 4.779\,\text{nH}$, $C_6 = 0.1219\,\text{pF}$, $R_6 = 1481\,\Omega$, $L_6 = 3.772\,\text{nH}$, $C_7 = 0.0669\,\text{pF}$, $R_7 = 2729\,\Omega$, $L_7 = 6.872\,\text{nH}$, $R_o = 12.8\,\Omega$, (b) Reflection losses of SAA simulated in CST MWS and reflection losses for ECM simulated in AWR-Microwave Office.

impedance BW is 1.08 GHz (6.91–7.99) GHz with a BW percentage of 14.49%. The CST MWS curve has another two -10 dB impedance BWs, which are 0.66 GHz (6.15–6.81) GHz with BW 10.18%, and (8.24–8.63) GHz with BW 4.62%. The AWR curve simulation resonates at 7.42 GHz with -10 dB impedance BW 0.82 GHz (7.02–7.84) GHz with BW 11.03%.

Generally, it can be seen from Fig. 14(b) that the two curves basically tally with one another at the main BW. The difference between the two curves is due to the numerical analysis in AWR Microwave Office, as some of the parameters have not been catered to, such as the effect of bending TL and the separation distance between two patches, which has a close relationship with mutual coupling and BW. The simulated results showed that the BW changed by changing the separation distance between elements. As mentioned earlier, in this design the separation distances are kept with R_{cc} 43.42 mm or r_{ee} 29.7 mm ($0.73\lambda_o$ at 7.419 GHz).

As aforementioned, there is a discontinuity between a patch and the feeding line, which is also observed with a sequential feeding network. This paper takes into consideration the discontinuity between adjacent transformers at the point where two branches meet. As shown in Fig. 15(a), there are two types of discontinuities; the first is along the spiral arches between transforms (T_2-T_4) and (T_4-T_6) which are represented by (2–4) and (4–6), while the second type is between transformers or feed lines (T_1, T_3, T_5, and T_7) with transformers (T_2, T_4, and T_6). These discontinuities between branches are represented by (1–2), (2–3), (3–4), (4–5), (5–6), and (6–7). It is observed from simulated results shown in Fig. 14(b) that discontinuities (2–3), (3–4), (4–5), (5–6), and (6–7) have no effect on improving the reflection loss of array, therefore can be neglected. The likely reason is owing to the thin width of transformers T_3, T_5, and T_6, and as evidence, the values of discontinuity (C_f, L_{f1}, and L_{f2}), which are calculated from (23), (26), and (27), do not depend on the frequency but depend on the width of TL. Further, the discontinuity (1–2) has a significant negative effect on the reflection loss of the array, although the width of T_1 is thin, and this is probably due to T_1 and T_2 being close to the input port. This increases the reflection loss if taken into account and, therefore, must be neglected. As a result, only two discontinuities will be considered: (2–4) and (4–6).

Figure 15(b) shows the same circuit model of the suggested array displayed before in Fig. 8(a) with the addition of the effect of the discontinuity between T_2–T_4 and T_4–T_6, represented by $C_{f(2\text{–}4)}$, $L_{f1(2\text{–}4)}$, $L_{f2(2\text{–}4)}$ and $C_{f(4\text{–}6)}$, $L_{f1(4\text{–}6)}$, $L_{f2(4\text{–}6)}$. Fig. 15(c) shows a comparison between AWR reflection losses for an array without and with calculating the effect of discontinuity between (T_2–T_4) and (T_4–T_6). However, calculating the effect of discontinuity will enhance the AWR curve by about 1.54 dB. The result of discontinuity shows that its effect is very low, and this is another proof of the work reported by Pozar and Schaubert in [37]. As mentioned earlier in the introduction, the series feed network is the best choice to reduce discontinuity [7].

4. MEASURED RESULTS

For validation purposes, the SAA prototype has been fabricated based on the geometrical dimensions displayed in Table 1 by chemical method, while cutting the edge of the prototype and drilling the main port (port 1) have been done using milling CNC machine. The substrate employed is Rogers RT/Duroid 5880, ($\varepsilon_r = 2.2$, loss tangent $= 0.009$, substrate thickness $= 1.575$ mm, and copper thickness $= 0.035\,\mu$m). The pro-

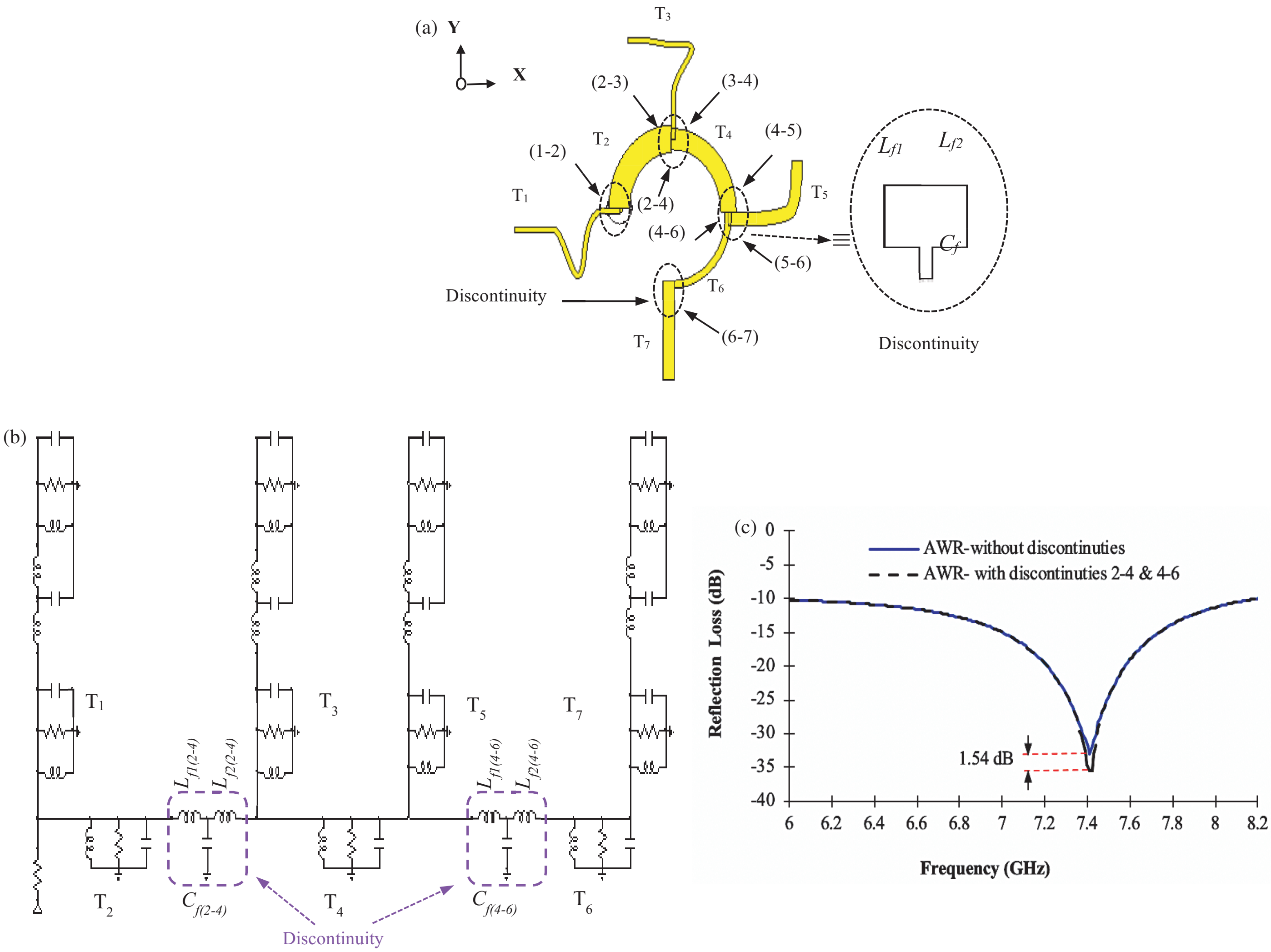

FIGURE 15. (a) The network discontinuity between transformers. (b) The ECM of SAA with consideration the discontinuity impact among T2–T4 and T4–T6, $L_{f1(2\text{–}4)} = 0.000014105$ pH, $L_{f2(2\text{–}4)} = 0.000016403$ pH, $C_{f(2\text{–}4)} = 0.000000010713$ pF, $L_{f1(4\text{–}6)} = 0.000061481$ pH, $L_{f2(4\text{–}6)} = 0.000089288$ pH, $C_{f(4\text{–}6)} = 0.000000017566$ pF. (c) Comparison between reflection losses of SAA simulated in CST MWS and reflection losses for ECM simulated in AWR-Microwave Office without discontinuity and with discontinuity between T (2–4) and T (4–6).

totype was experimentally tested at the Universiti Technical Malaysia Melaka employing a vector network analyser, Agilent N5242A, for measuring reflection loss. Fig. 16 shows a photograph of the SAA fabricated prototype. The measurement was implemented using a high-precision test cable with 3.5 mm precision connectors. The analyzer was calibrated employing the Agilent N4433A calibration kit.

The reflection loss, AR, and gain simulated and measured results are demonstrated in Figs. 17(a), (b), and (c), respectively. The -10 dB reflection loss realizes the simulated BW from (6.14–8) GHz, and measured BW from (6.15–8.23) GHz, as seen in Fig. 17(a). Fig. 17(b) illustrates the measured and simulated AR results. The measured -3 dB AR BW (6.2–7.8) GHz is approximately 22.85%, within the -10 dB coefficient reflection BW. The variation between measurement and simulation is the reason for manufacturing and measurement inaccuracy, as well as due to the uncertain relative permittivity of the board. Fig. 17(c) presents the simulated and measured gains. It is observed that the measured gain of the SAA is around (7.6–10.2) dBi within the 3 dB AR BW. The gain variation within AR BW is smaller than 2.8 dBi, where the measured maximum gain is around 10.2 dBi at 7.4 GHz. Fig. 18 displays the measured normalized and simulated radiation patterns in the Phi $=0$ and Phi $=90$ plane at frequencies 6.08 GHz and 7.43 GHz. During the measurement process, the impacts of the foam rack and tapes behind the antenna array may cause a few ripples in the recorded patterns.

Finally, to highlight the benefits of this study, Table 4 compares various antenna arrays utilizing the sequential feed network. The table compares the proposed work with previous research on impedance bandwidth, AR BW, gain, size, and substrate type (ε_r). Based on the table, the proposed antenna occupies 90.73, 58.13, 88.56, and 98.68 percent less space than [3, 21, 22, 24], respectively. In comparison to other works,

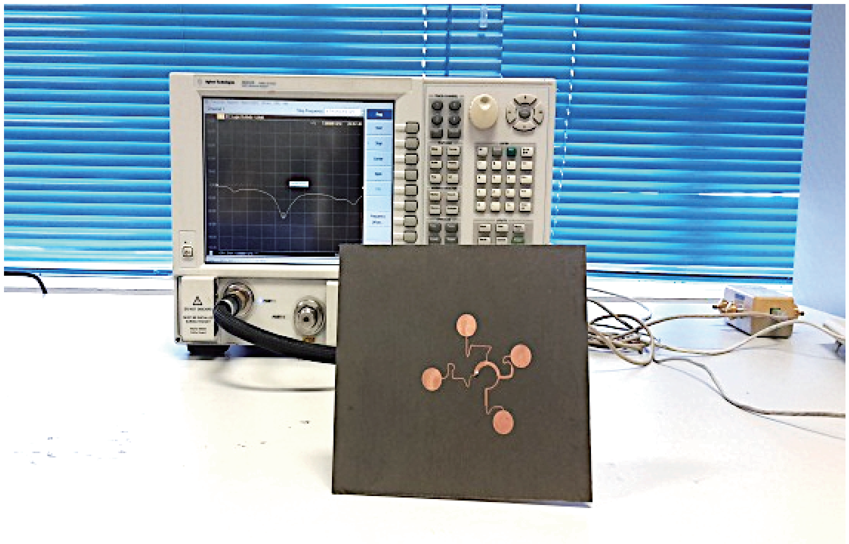

FIGURE 16. An image depicting the SAA being tested within the measurement setup.

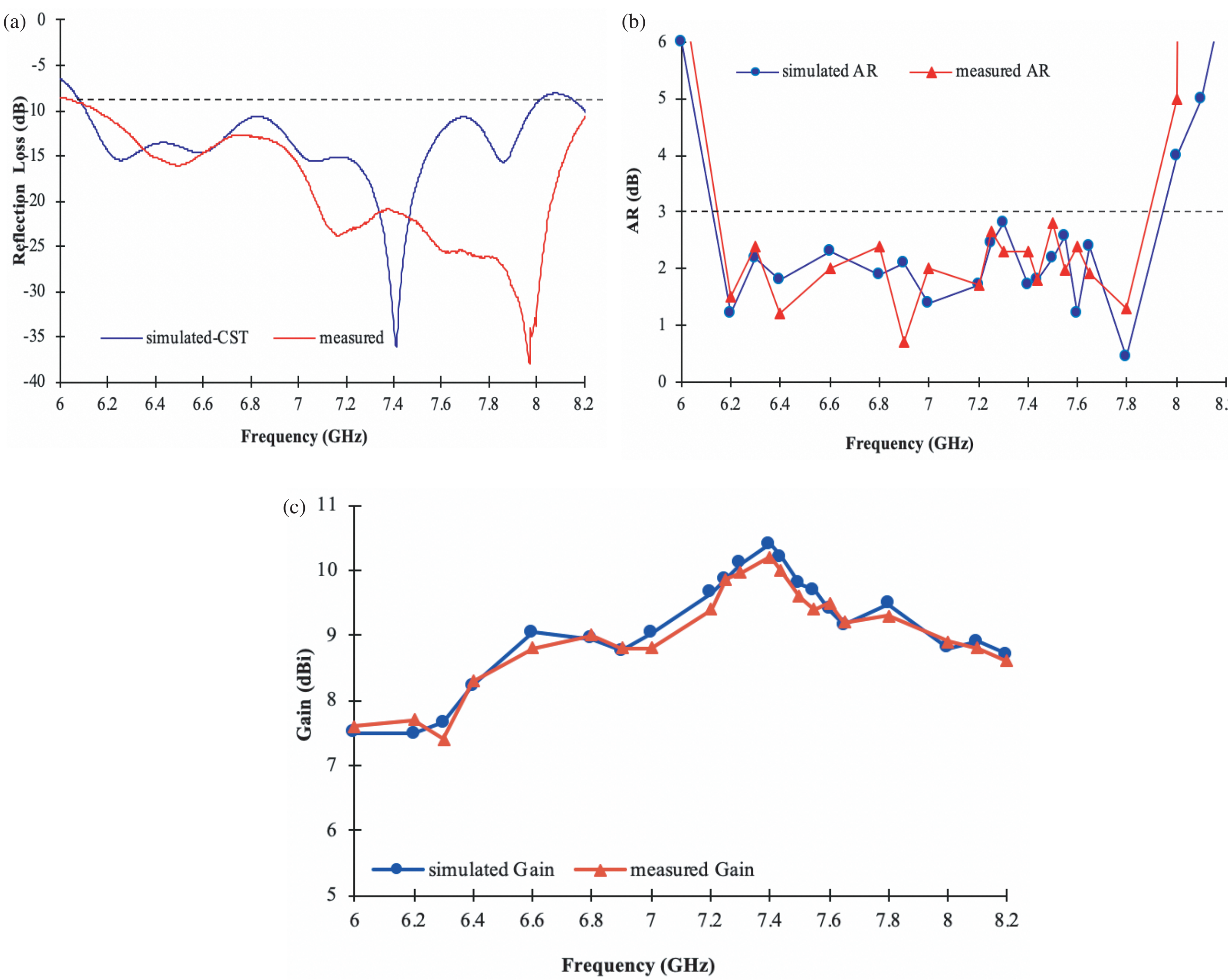

FIGURE 17. Simulated and measured (a) reflection loss BW, (b) AR BW, (c) gain.

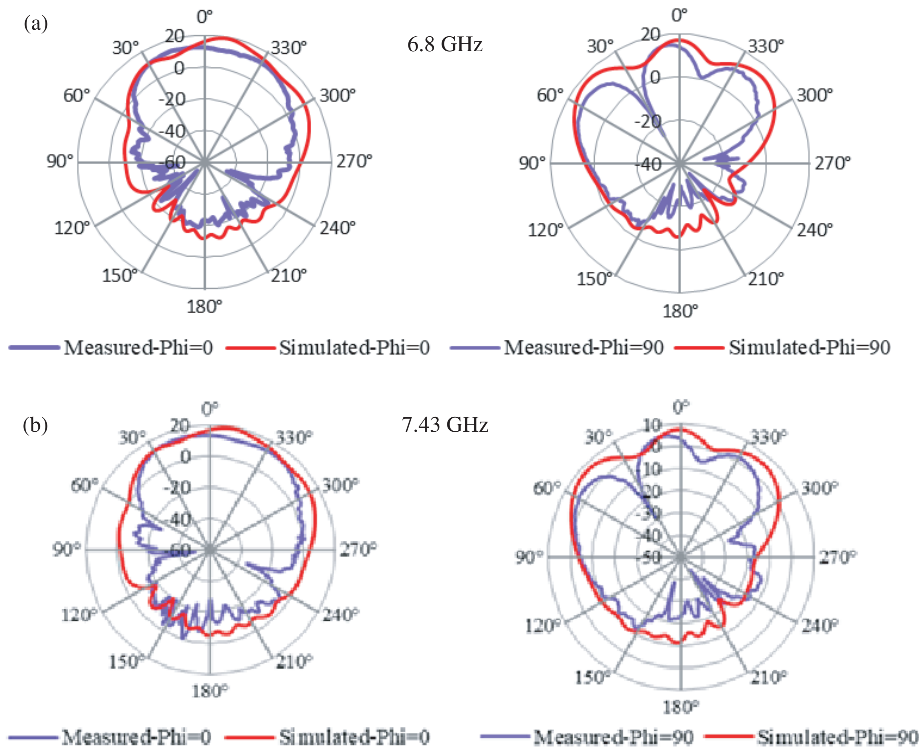

FIGURE 18. Measured normalized and Simulated radiation patterns of SAA. (a) 6.8 GHz. (b) 7.43 GHz.

TABLE 4. Comparison of the proposed structure with the similar designs in literature.

Ref.	IBW (GHz)	ARBW (GHz)	Peak gain (dBi)	Size (mm^3)	Substrate ε_r	Substrate type	Feed network type
[3]	3.96 (4.18–8.14)	3.04 (4.08–7.12)	10.84	$97 \times 112 \times 8.8 = 95603$	4.4	FR4	Sequential rotation
[20]	1.20 (5.10–6.30)	0.9 (5.32–6.22)	8.2	$45 \times 45 \times 1.6 = 3.240$	3.65	FR408	Sequential rotation
[21]	2.2 (4.8–7)	1.27 (5–6.27)	4.95–5.94	$92 \times 92 \times 2.5 = 21160$	3.5	NG	Sequential rotation
[22]	0.8 (1.15–1.95)	0.8 (1.15–1.90)	~ 8	$220 \times 220 \times 1.6 = 77440$	4.4	FR4	Sequential rotation
[23]	2.8 (4.0–6.8)	1.9 (5.1–7.0)	7.5	$92 \times 92 \times 0.8 = 6771.2$	4.4	FR4	Sequential rotation
[24]	0.7 (2.12–2.82)	0.6 (2.24–2.84)	~ 13.5	$205 \times 205 \times 16 = 672400$	4.4	FR4	Sequential rotation
This work	2.08 (6.15–8.23)	1.6 (6.2–7.8)	10.2	$75 \times 75 \times 1.575 = 8859$	2.2	Rogers	Sequential rotation

the impedance bandwidths and AR are superior to [20, 22, 24]. Also, it is clear that the suggested antenna's peak gain is adequate and greater than [21, 22], as shown in the table, despite their size being more significant than the proposed antenna; perhaps the difference is due to the spiral antenna array design. Moreover, the difference in gain is slight compared to [3], while the array size in [3] is 90.73% greater than the suggested antenna.

5. CONCLUSION

In this article, a spiral array antenna (SAA) with 2×2 circularly polarized (CP) spiral sequential feed network (SSFN) is presented for C-band applications. The ECM of the SAA with SSFN was proposed, and their performance was verified using CST and AWR software. The suggested SAA with 2×2 CP SSFN is designed and experimented with close correspondence between the simulated and measured outcomes, validated through a high-gain antenna and -3 dB of axial ratio. The tested results indicated that the net bandwidth of 2.08 GHz was covered (6.15–8.23 GHz). Also, the proposed antenna's axial ratio (AR) covered a bandwidth of 1.6 GHz (6.2–7.8) GHz, approximately 22.85% of the whole bandwidth. The proposed array antenna achieved a peak gain of 10.2 dBi at 7.43 GHz.

ACKNOWLEDGEMENT

The authors wish to express their profound gratitude to Universiti Teknikal Malaysia Melaka (UTeM) for their generous support. This work was made possible through the grant PJP/2024/FTKEK/PERINTIS/S01388. Their assistance and resources have been instrumental in the successful completion of this research.

REFERENCES

[1] Al-Gburi, A. J. A., Z. Zakaria, H. Alsariera, M. F. Akbar, I. M. Ibrahim, K. S. Ahmad, S. Ahmad, and S. S. Al-Bawri, "Broadband circular polarised printed antennas for indoor wireless communication systems: A comprehensive review," *Micromachines*, Vol. 13, No. 7, 1048, 2022.

[2] Siahcheshm, A., J. Nourinia, and C. Ghobadi, "Circularly polarized antenna array with a new sequential phase feed network utilizing directional coupler," *AEU — International Journal of Electronics and Communications*, Vol. 93, 75–82, 2018.

[3] Siahcheshm, A., J. Nourinia, C. Ghobadi, M. Karamirad, and B. Mohammadi, "A broadband circularly polarized cavity-backed archimedean spiral array antenna for C-band applications," *AEU — International Journal of Electronics and Communications*, Vol. 81, 218–226, 2017.

[4] Ahmad, K. S., F. C. Seman, and S. A. Hamzah, "Dual microstrip antenna patches with orthogonal i-shaped defected ground structure for beam steering realization," *2016 IEEE Asia-Pacific Conference on Applied Electromagnetics (APACE)*, 174–178, 2016.

[5] Ahmad, K. S., M. Z. A. A. Aziz, and N. B. Abdullah, "Microstrip antenna array with defected ground structure and copper tracks for bandwidth enhancement," in *2020 IEEE International RF and Microwave Conference (RFM)*, 1–5, Kuala Lumpur, Malaysia, 2020.

[6] Hall, P. S. and C. M. Hall, "Coplanar corporate feed effects in microstrip patch array design," *IEE Proceedings H (Microwaves, Antennas and Propagation)*, Vol. 135, No. 3, 180–186, 1988.

[7] Jazi, M. N. and M. N. Azarmanesh, "Design and implementation of circularly polarised microstrip antenna array using a new serial feed sequentially rotated technique," *IEE Proceedings — Microwaves, Antennas and Propagation*, Vol. 153, No. 2, 133–140, 2006.

[8] Ta, S. X. and I. Park, "Compact wideband circularly polarized patch antenna array using metasurface," *IEEE Antennas and Wireless Propagation Letters*, Vol. 16, 1932–1936, 2017.

[9] Chu, J.-Y., L. Peng, X.-F. Li, and X. Jiang, "Archimedean spiral antenna loaded by frequency selective surface," *Progress In Electromagnetics Research M*, Vol. 95, 199–209, 2020.

[10] Supreeyatitikul, N., D. Torrungrueng, and C. Phongcharoenpanich, "Quadri-cluster broadband circularly-polarized sequentially-rotated metasurface-based antenna array for C-band satellite communications," *IEEE Access*, Vol. 9, 67 015–67 027, 2021.

[11] Xie, J.-Y., L. Peng, B.-J. Wen, and X. Jiang, "Archimedean spiral antenna with two opposite uni-directional circularly polarized radiation bands designed by resonance based reflectors," *Progress In Electromagnetics Research Letters*, Vol. 70, 23–30, 2017.

[12] Inserra, D., W. Hu, and G. Wen, "Design of a microstrip series power divider for sequentially rotated nonuniform antenna array," *International Journal of Antennas and Propagation*, Vol. 2017, No. 1, 9482979, 2017.

[13] Maddio, S., "A compact two-level sequentially rotated circularly polarized antenna array for C-band applications," *International Journal of Antennas and Propagation*, Vol. 2015, No. 1, 830920, 2015.

[14] Deng, C., Y. Li, Z. Zhang, and Z. Feng, "A wideband sequential-phase fed circularly polarized patch array," *IEEE Transactions on Antennas and Propagation*, Vol. 62, No. 7, 3890–3893, 2014.

[15] Hall, P. S., J. S. Dahele, and J. R. James, "Design principles of sequentially fed, wide bandwidth, circularly polarised microstrip antennas," *IEE Proceedings H (Microwaves, Antennas and Propagation)*, Vol. 136, No. 5, 381–389, 1989.

[16] Smith, M. S. and P. S. Hall, "Analysis of radiation pattern effects in sequentially rotated arrays," *IEE Proceedings — Microwaves, Antennas and Propagation*, Vol. 141, No. 4, 313–320, 1994.

[17] Chen, A., Y. Zhang, Z. Chen, and S. Cao, "A Ka-band high-gain circularly polarized microstrip antenna array," *IEEE Antennas and Wireless Propagation Letters*, Vol. 9, 1115–1118, 2010.

[18] Chen, A., Y. Zhang, Z. Chen, and C. Yang, "Development of a Ka-band wideband circularly polarized 64-element microstrip antenna array with double application of the sequential rotation feeding technique," *IEEE Antennas and Wireless Propagation Letters*, Vol. 10, 1270–1273, 2011.

[19] Jalili, F., J. Pourahmadazar, J. Nourinia, and V. Rafii, "Circularly polarized circular slot antenna array using sequentially rotated feed network," *Journal of Communication Engineering*, Vol. 1, No. 1, 38–46, 2016.

[20] Maddio, S., "A compact wideband circularly polarized antenna array for C-band applications," *IEEE Antennas and Wireless Propagation Letters*, Vol. 14, 1081–1084, 2015.

[21] Zheng, Q., C. Guo, G. A. E. Vandenbosch, and J. Ding, "Low-profile circularly polarized array with gain enhancement and RCS reduction using polarization conversion EBG structures," *IEEE Transactions on Antennas and Propagation*, Vol. 68, No. 3, 2440–2445, 2020.

[22] Fu, S., S. Fang, Z. Wang, and X. Li, "Broadband circularly polarized slot antenna array fed by asymmetric CPW for L-band applications," *IEEE Antennas and Wireless Propagation Letters*, Vol. 8, 1014–1016, 2009.

[23] Rafii, V., J. Nourinia, C. Ghobadi, J. Pourahmadazar, and B. S. Virdee, "Broadband circularly polarized slot antenna array using sequentially rotated technique for C-band applications," *IEEE Antennas and Wireless Propagation Letters*, Vol. 12, 128–131, 2013.

[24] Jiang, X., Z. Zhang, Y. Li, and Z. Feng, "A low-cost wideband circularly polarized slot array with integrated feeding network and reduced height," *IEEE Antennas and Wireless Propagation Letters*, Vol. 15, 222–225, 2015.

[25] Rupčić, S. and V. Mandrić, "Spiral antenna array configurations on spherical surface," in *ICECom 2013*, 1–5, Dubrovnik, Croatia, 2013.

[26] Gao, S., Y. Qin, and A. Sambell, "Low-cost broadband circularly polarized printed antennas and array," *IEEE Antennas and Propagation Magazine*, Vol. 49, No. 4, 57–64, 2007.

[27] Evans, H., P. Gale, B. Aljibouri, E. G. Lim, E. Korolkeiwicz, and A. Sambell, "Application of simulated annealing to design of serial feed sequentially rotated 2 × 2 antenna array," *Electronics Letters*, Vol. 36, No. 24, 1987–1988, 2000.

[28] Subhi, K., F. C. Seman, S. A. Hamzah, G. C. Hock, and S. M. Shah, "Circuit model for microstrip array antenna with defected ground structures for mutual coupling reduction and beamforming applications," *International Journal of Integrated Engineering*, Vol. 13, No. 1, 101–119, 2021.

[29] Shang, X. and M. J. Lancaster, "Patch antenna with integrated bandpass filter," in *4th Annual Seminar on Passive RF and Microwave Components*, 17–21, Birmingham, UK, 2013.

[30] Chen, A., Y. Zhang, Z. Chen, and C. Yang, "Development of a Ka-band wideband circularly polarized 64-element microstrip antenna array with double application of the sequential rotation feeding technique," *IEEE Antennas and Wireless Propagation Letters*, Vol. 10, 1270–1273, 2011.

[31] Singh, A. K., R. K. Gangwar, and B. K. Kanaujia, "Wideband and compact slot loaded annular ring microstrip antenna using L-probe proximity-feed for wireless communications," *International Journal of Microwave and Wireless Technologies*, Vol. 8, No. 7, 1085–1093, 2016.

[32] Sagiroglu, S. and A. Kalinli, "Determining resonant frequencies of various microstrip antennas within a single neural model trained using parallel tabu search algorithm," *Electromagnetics*, Vol. 25, No. 6, 551–565, 2005.

[33] Ray, K. P. and G. Kumar, "Determination of the resonant frequency of microstrip antennas," *Microwave and Optical Technology Letters*, Vol. 23, No. 2, 114–117, 1999.

[34] Garg, R., *Microstrip Antenna Design Handbook*, Artech House, 2001.

[35] Badjian, M. H., C. K. Chakrabarty, S. Devkumar, and G. C. Hock, "Lumped element circuit model approximation of an UWB patch antenna," in *2009 IEEE 9th Malaysia International Conference on Communications (MICC)*, 28–32, Kuala Lumpur, Malaysia, 2009.

[36] Hong, J.-S. G. and M. J. Lancaster, *Microstrip Filters for RF/microwave Applications*, John Wiley & Sons, 2004.

[37] Pozar, D. M. and D. H. Schaubert, "Comparison of three series fed microstrip array geometries," in *Proceedings of IEEE Antennas and Propagation Society International Symposium*, 728–731, Ann Arbor, MI, USA, 1993.